Vol. 697: 1–13, 2022
https://doi.org/10.3354/meps14151

MARINE ECOLOGY PROGRESS SERIES
Mar Ecol Prog Ser

Published September 22

Baltic Sea transparency from ships and satellites: centennial trends

Mati Kahru[1,*], Henry Bittig[2], Ragnar Elmgren[3], Vivi Fleming[4], Zhongping Lee[5], Gregor Rehder[2]

[1]Scripps Institution of Oceanography, UCSD, La Jolla, CA 92092-0218, USA
[2]Leibniz Institute for Baltic Sea Research Warnemünde (IOW), Seestrasse 15, 18119 Rostock, Germany
[3]Department of Ecology, Environment and Plant Sciences, Stockholm University, 10691 Stockholm, Sweden
[4]SYKE Marine Research Centre, PO Box 140, 00251 Helsinki, Finland
[5]School for the Environment, University of Massachusetts Boston, Boston, MA 02125, USA

ABSTRACT: Water transparency can be measured with optical instruments and estimated with satellite sensors, but such measurements have been widely available for only a few decades. Estimates of water transparency using a white disk called a Secchi disk have been made for over a century and can be used to estimate long-term trends. However, historic *in situ* measurements of the Secchi depth (Z_{Sd}) were irregular in space and time and are difficult to interpret in regular time series due to biases introduced by changing locations and the timing of measurements. Satellite data time series, on the other hand, have consistent resolution in both space and time but cover too short a time to resolve climate-scale trends. We normalized historic Z_{Sd} measurements in the Baltic Sea with a satellite-derived mean climatology at 5 d temporal and 4 km spatial resolutions and created a merged time series of Z_{Sd} for the last century. The mean Z_{Sd} in the Baltic Sea from 1927–2020 decreased by 4.2 ± 0.6 m at a rate of 0.045 ± 0.06 m yr^{-1}. Most of the change happened before 1987, and a further decrease was evident primarily in the satellite data during the 1998–2008 period. After 2008, no significant trend in Z_{Sd} and or the coefficient of diffuse light attenuation was detected in the Baltic Sea. However, in some sub-basins of the Baltic Sea, the decrease in Z_{Sd} continued even after that. The decrease in spectral water transparency in recent decades was highest in the 412 nm band, indicating an increase in the concentration of chromophoric dissolved organic matter.

KEY WORDS: Water transparency · Baltic Sea · Eutrophication · Secchi depth · Light attenuation · k_d490 · CDOM · Chromophoric dissolved organic matter · Climate variability

1. INTRODUCTION

The Baltic Sea is a large, semi-enclosed sea that has been under intense anthropogenic influence for many decades. Signs of offshore eutrophication, such as increased nutrient concentrations, were recognized in the Baltic Sea as early as the 1960s (e.g. Fonselius 1969, Elmgren 1989, Savchuk 2018). Even though the Baltic Sea is one of the best studied oceanographic regions in the world, most historic ship-based measurements were sporadic, sparse in space, and too infrequent to resolve the natural variability. Water transparency is an important ecological variable that directly affects processes such as primary production, solar bleaching of organic material, phytoplankton physiology, and behavior of zooplankton and fish. Water transparency can be measured with optical instruments and estimated with satellite sensors, but has also been estimated for over a century by using a simple white disk (Preisendorfer

*Corresponding author: mkahru@ucsd.edu

Publisher: Inter-Research · www.int-res.com

1986, Aarup 2002). The depth of disappearance of the disk is called the Secchi depth (Z_{Sd}). While Z_{Sd} is a rather crude measurement, its advantage is the large number of measurements available, going back over 100 yr. Several previous studies (Launiainen et al. 1989, Sandén & Håkansson 1996, Fleming-Lehtinen & Laamanen 2012, Dupont & Aksnes 2013) have shown that the water transparency in the Baltic measured with Z_{Sd} has decreased significantly in recent decades. However, shipborne measurements were always sporadic and inconsistent in space and time and the variability in measured Z_{Sd} is huge. Water transparency is sporadically reduced by river outflow plumes, particle resuspension events near the coasts and on shallow off-shore banks, and phytoplankton blooms. Quasi-regular events such as the phytoplankton spring bloom and the cyanobacteria summer bloom also severely curtail Z_{Sd}. All these events typically last from days to weeks or even longer. Dupont & Aksnes (2013) fitted an empirical relationship between Z_{Sd} and the distance to coast and bottom depth and removed the mean effect of those variables from Z_{Sd}. However, these effects are not spatially or temporally uniform. Seasonal effects caused by quasi-regular events such as the phytoplankton spring bloom and the cyanobacteria summer bloom clearly affect water transparency (e.g. Kahru & Elmgren 2014, Kahru et al. 2016a). Here, we removed both the mean spatial and seasonal variability in Z_{Sd} by subtracting satellite-derived mean Z_{Sd} climatology from individual *in situ* Z_{Sd} measurements. Satellite data time series have high and consistent resolution in both space and time but are too short to resolve climate-scale variability. We used satellite-derived mean Z_{Sd} climatology at 5 d temporal and 4 km spatial resolutions and normalized historic Z_{Sd} measurements by subtracting the seasonal (with 5 d resolution) mean value of the nearest 4 km pixel from each *in situ* Z_{Sd} measurement. We then compared *in situ* and satellite time series and merged them. The goal of this study was to create the best possible time series of Z_{Sd} using historic *in situ* measurements and modern era satellite measurements.

2. DATA AND METHODS

2.1. Satellite data

A number of models exist for calculating Z_{Sd} from optical inputs (e.g. Alikas & Kratzer 2017) but most are empirical in nature, which makes them less applicable to measurements not covered by the data sets used in the development of the algorithm. The algorithm of Lee et al. (2015), on the other hand, is based on a revised model of Z_{Sd} theory and adapts to the change in the spectral composition of light. It derives the Z_{Sd} at the estimated transparent window of the water column. Theoretical predictions of the model have been validated with Z_{Sd} measurements for over 90 yr (Lee et al. 2018).

The primary source of satellite data used here was the ESA Ocean Colour Climate Change Initiative (OC-CCI) version 5.0 (Sathyendranath et al. 2019; https://esa-oceancolour-cci.org/). OC-CCI data are available from September 1997 to the end of June 2020 and are merged from multiple ocean color sensors: SeaWiFS (1997–2010), MERIS (2002–2012), MODIS-Aqua (2002–2020), VIIRS-SNPP (2012–2020), and OLCI-A (2017–2020). The main goal of the ESA-CCI data set was to produce a compatible time series by removing inter-sensor differences. Time series from individual sensors cover only portions of the whole time series, are often processed with different methods, and are less suitable for estimating long-term trends. At high latitudes, ocean color data cannot be obtained during the winter season due to the low sun elevation (Kahru et al. 2016b). Frequent cloud cover further reduces the availability of ocean color data. Therefore, north of the southernmost Baltic, satellite ocean color data are not available for the winter season. In ocean optics, the common measure of water transparency is the coefficient of diffuse light attenuation at 490 nm (k_d490). This is also a standard product in many satellite data sets, including OC-CCI. We applied the Lee et al. (2015) Z_{Sd} algorithm to OC-CCI daily remote sensing reflectance data sets of the 6 spectral bands (412, 443, 490, 510, 560, 665 nm) at about 4.5 km spatial resolution. As part of the Lee et al. (2015) algorithm, we computed the coefficient of diffuse light attenuation (k_d) for the 6 spectral bands at the same spatial and temporal resolutions and found the spectral band with minimal k_d. The calculations were implemented in the application 'wam_zsd', which is part of the 'Wimsoft' package (https://www.wimsoft.com/). We also evaluated the empirical Alikas & Kratzer (2017) Baltic Z_{Sd} algorithm against *in situ* Z_{Sd} data, but it appeared less accurate in retrievals and was therefore not used further.

2.2. *In situ* data

Aarup (2002) and Fleming-Lehtinen & Laamanen (2012) assembled data sets consisting of tens of thou-

sands of *in situ* Z_{Sd} measurements from both the North and Baltic Seas for 1903–2009. Additional Z_{Sd} measurements were extracted from ICES and other sources until early 2016 (HELCOM 2018). A relatively small number of measurements (332 out of 28 141) missed the day of the month and were assigned the middle day of the respective month. This change did not have any significant effects on the results. Early Z_{Sd} measurements were made using a viewer (see Fig. 2 in Fleming-Lehtinen & Laamanen 2012), while measurements from 1957 onward were not. Following Fleming-Lehtinen & Laamanen (2012), the early data were transformed with a simple empirical correction according to the formula proposed by Launiainen et al. (1989).

In situ Z_{Sd} measurements were converted to Z_{Sd} anomalies by subtracting the satellite-derived mean Z_{Sd} value (1997–2020) of the nearest pixel on a 4 km grid of the respective 5 d period of the annual cycle (see Section 2.3). As satellite data are unreliable adjacent to the coast, we used the HELCOM open-sea regions (Table 1, Fig. 1) that exclude coastal areas approximately 4 km from the coast. This division was also used by Fleming-Lehtinen & Laamanen (2012). The number of available *in situ* Z_{Sd} anomalies was also reduced by the lack of corresponding satellite data during the winter season due to low sun elevation and/or persistent cloudiness. The total number of *in situ* Z_{Sd} measure-

Table 1. HELCOM open-sea regions and the number of *in situ* Secchi depth (Z_{Sd}) measurements converted to Z_{Sd} anomaly. See Fig. 1 for a map

HELCOM ID	Assessment unit	Code	No. of Secchi measurements
SEA-001	Kattegat	KAT	4477
SEA-002	Great Belt	B	725
SEA-003	The Sound	S	134
SEA-004	Kiel Bay	KB	687
SEA-005	Bay of Mecklenburg	BM	738
SEA-006	Arkona Basin	AB	2667
SEA-007	Bornholm Basin	BB	4329
SEA-008	Gdansk Basin	GD	1284
SEA-009	Eastern Gotland Basin	EGB	3258
SEA-010	Western Gotland Basin	WGB	1953
SEA-011	Gulf of Riga	GR	1552
SEA-012	Northern Baltic Proper	NBP	960
SEA-013A	Gulf of Finland Western	GFW	904
SEA-013B	Gulf of Finland Eastern	GFE	708
SEA-014	Åland Sea	AS	1805
SEA-015	Bothnian Sea	BS	195
SEA-016	The Quark	Q	1183
SEA-017	Bothnian Bay	BBay	582
Total			28141

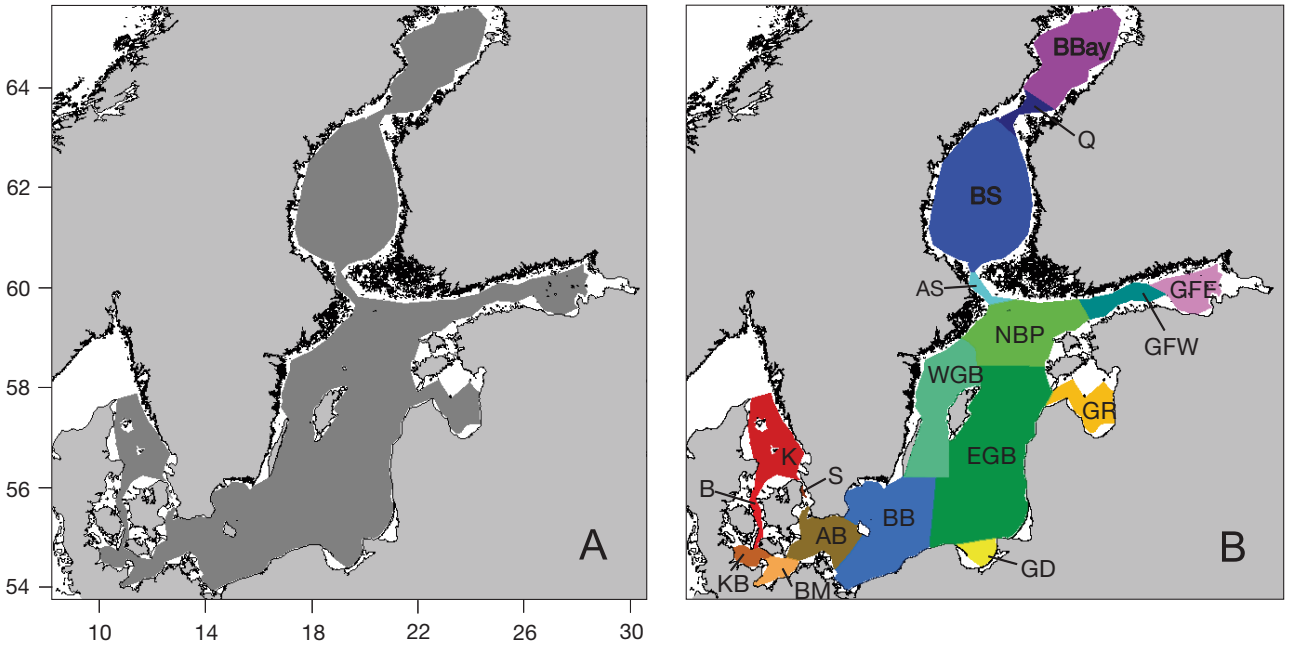

Fig. 1. Study areas in the Baltic Sea showing (A) the entire Baltic Sea HELCOM open sea area (dark gray) and (B) the 18 subregions: Kattegat (K), Great Belt (B), The Sound (S), Kiel Bay (KB), Bay of Mecklenburg (BM), Arkona Basin (AB), Bornholm Basin (BB), Gdansk Basin (GD), Eastern Gotland Basin (EGB), Western Gotland Basin (WGB), Gulf of Riga (GR), Northern Baltic Proper (NBP), Gulf of Finland Western (GFW), Gulf of Finland Eastern (GFE), Åland Sea (AS), Bothnian Sea (BS), the Quark (Q), and Bothnian Bay (BBay)

ments converted to Z_{Sd} anomalies during 1903–2016 was reduced from 37 491 to 28 141 by excluding measurements from coastal zones and those with no matching satellite 5 d climatology value. The spatial and temporal distributions of these data were uneven (Fig. 2), with a major gap from 1940 to 1956. Individual Z_{Sd} anomaly values were pooled over monthly and annual periods.

Time series of the mean, median, and other statistics were calculated for the whole Baltic Sea and each of the 18 regions (Table 1, Fig. 1B), with an emphasis on the annual time series.

2.3. Normalization of Z_{Sd} data

Satellite measurements over more than 23 yr (1997–2020) were used to create Z_{Sd} and k_d mean climatologies (i.e. mean seasonal cycles) with 5 d temporal and 4.5 km spatial resolution. Daily data sets were composited over 5 d periods by averaging valid pixel values (i.e. the composited value is the mean of 1–5 valid values). During cloudy periods that still left many missing pixel values, missing pixels in 5 d composites with valid values in the previous and following 5 d composites were filled with linear interpolation. Corresponding 5 d periods over all available years were averaged to produce mean maps of satellite-derived Z_{Sd} for each of the 73 five-day periods over 1 yr. These 73 data sets, therefore, consist of the mean pixel values for year days 1–5, 6–10, 11–15, etc. The mean annual cycle for each pixel is made up of the 73 five-day values. However, due to low sun elevation in winter and persistent cloudiness, some of the winter 5 d climatology values were missing. The median number of valid climatology values for the whole Baltic Sea was 57 (63 after interpolation) and decreased from south to north. As mentioned in Section 2.2, due to the missing satellite climatology values in winter, the number of calculated Z_{Sd} anomaly values was reduced compared to the number of available *in situ* measurements.

Anomalies of *in situ* Z_{Sd} were created by subtracting the respective climatology value of the nearest pixel in space and the nearest 5 d period corresponding to the date of the measurement. This normalization of the numerous but spatially and temporally irregular historic samples from Z_{Sd} to Z_{Sd}-anomaly made measurements in different areas (with different means) more comparable. The same procedure was applied to satellite data by subtracting the climatology value from the 5 d Z_{Sd} composites. *In situ* Z_{Sd} anomalies and 5 d satellite Z_{Sd} anomalies were averaged over monthly and annual periods to obtain annual Z_{Sd} anomalies for each of the 18 regions and the whole study area.

A piecewise linear fit routine with automated breakpoint detection following Owens & Wong (2009) and Cabanes et al. (2016) was applied to the Z_{Sd} anomaly time series for the entire Baltic Sea.

3. RESULTS

3.1. Validation of satellite estimates

The Lee et al. (2015) Z_{Sd} model has been applied in a number of regions (e.g. Shang et al. 2016, Liu et al. 2020a,b). We did not attempt a rigorous verification with high-resolution satellite match-ups within a short period (e.g. 1 h). Instead, we performed a general validation of the satellite Z_{Sd} data sets at daily and 4.5 km resolutions. We recognize that there can be considerable variability within each 4.5 km pixel. We found 3130 same-day matchups and used the average pixel value in a 3 × 3 pixel window centered at the *in situ* measurement. Match-ups with high pixel-to-pixel variability [(max. – min.) / min. > 0.5)] and less than 5 valid pixels out of 9 were excluded. The accuracy of the satellite estimates was quite good (R^2 = 0.61; Fig. 3A) considering the pixel-to-pixel and within-pixel variability. Subsets of match-ups in each of the 18 sub-areas showed no evidence for differences in the relationships (Fig. 3C,D). As the independent variable (*in situ* Z_{Sd}) is also known with an error, the relationships between *in situ* and satellite Z_{Sd} (Fig. 3) were evaluated using both the ordinary least squares (OLS) linear regression and a Type II reduced major axis linear regression (York et al. 2004). While the OLS regression was always <1, overestimation at the low end and underestimation at the high end are expected due to the spatial averaging of small-scale extremes by the bigger footprint of satellite measurements. We conclude that satellite estimates of Z_{Sd} are reasonably accurate estimates of *in situ* Z_{Sd}.

3.2. Satellite time series of k_d490 and Z_{Sd} for the whole Baltic Sea region

Averaged over the whole Baltic Sea area (Fig. 1A), the satellite-derived time series showed an increasing trend in k_d490 and a decreasing trend in Z_{Sd} (Fig. 4). The slope of the trend over the 1998–2020

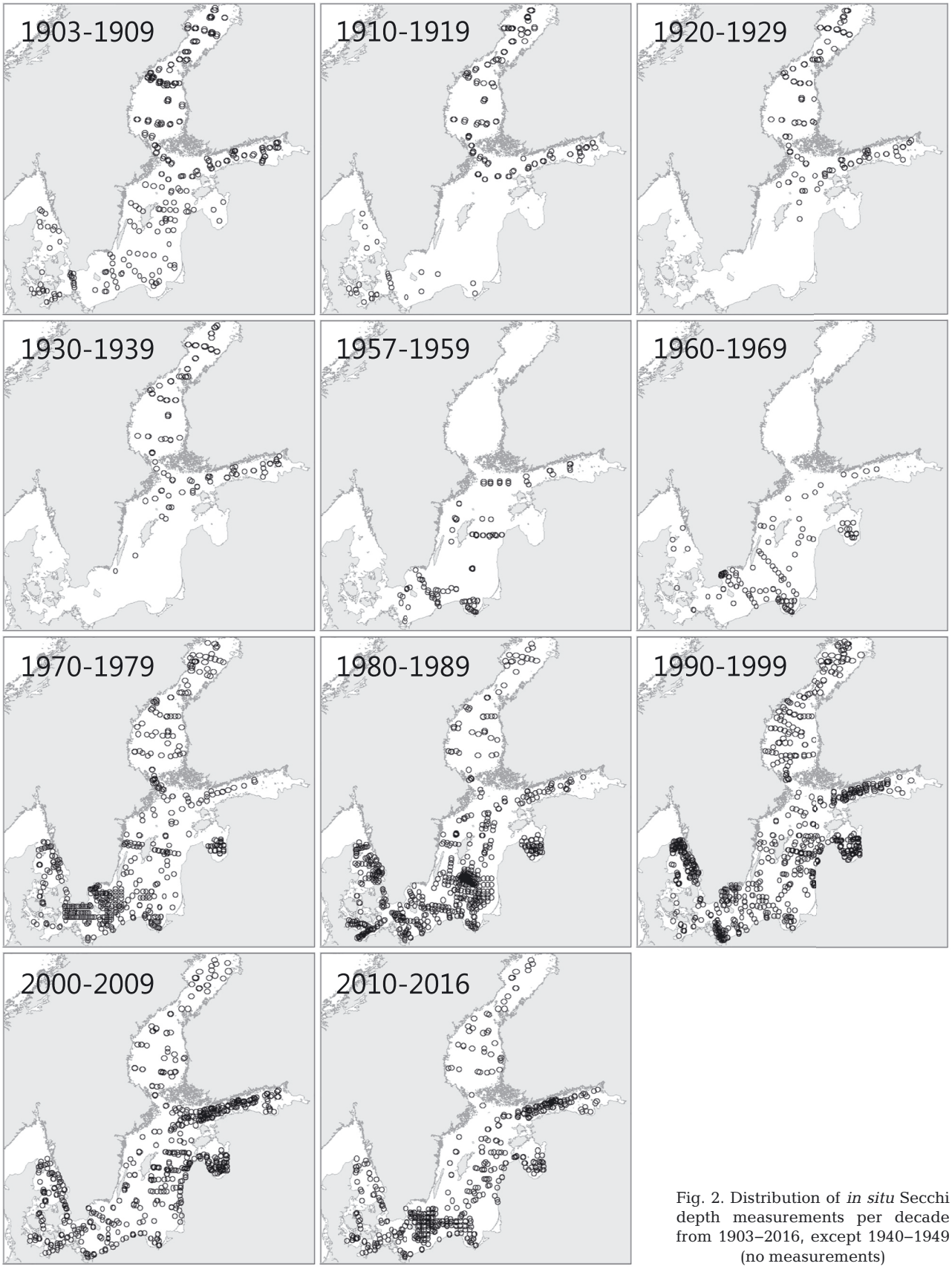

Fig. 2. Distribution of *in situ* Secchi depth measurements per decade from 1903–2016, except 1940–1949 (no measurements)

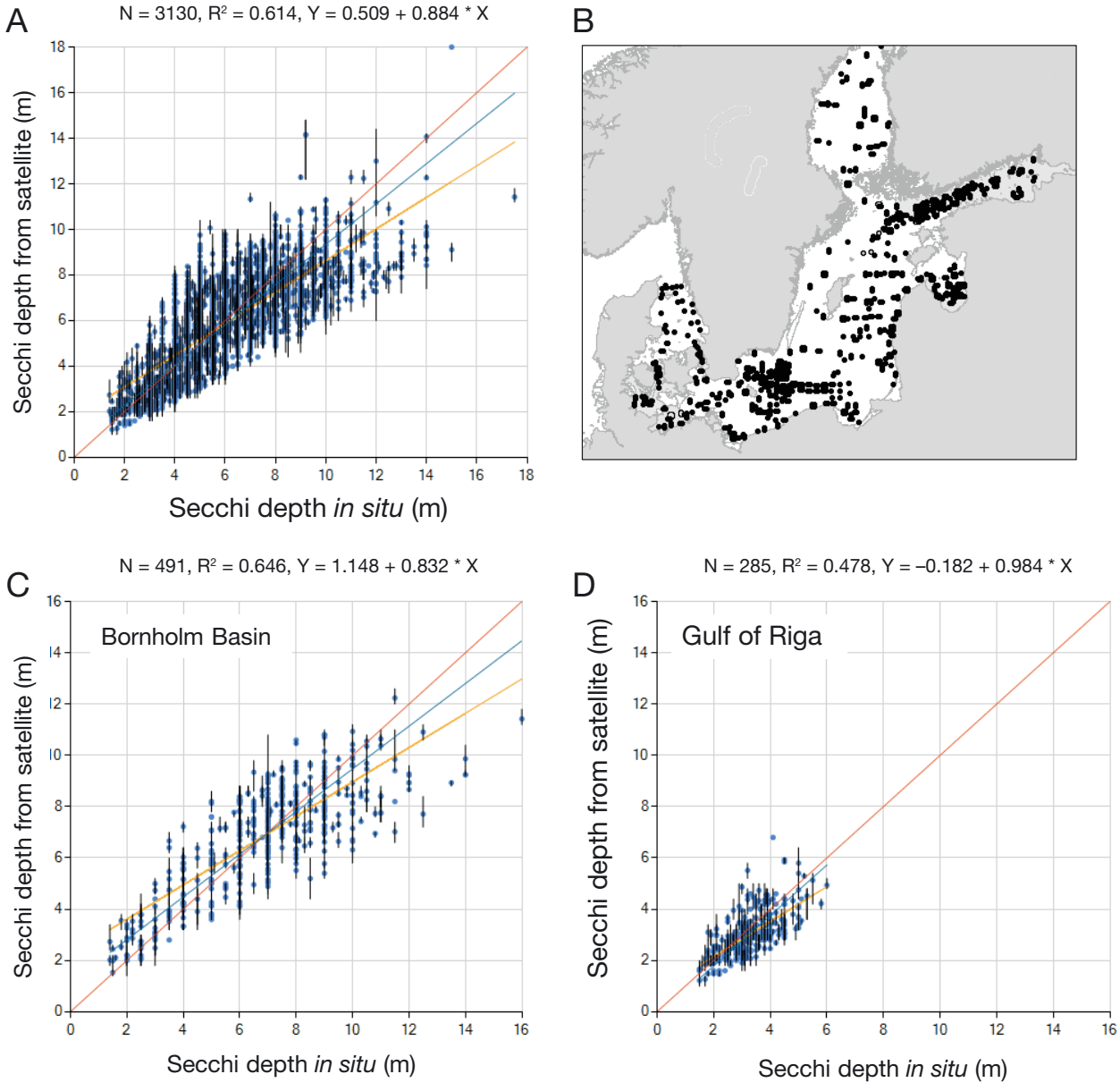

Fig. 3 (A) Match-ups of satellite-derived Secchi depths (Lee et al. 2015 algorithm) against same-day *in situ* measurements. Small, filled circles: means; vertical lines: range of values in a 3 × 3 pixel area corresponding to the *in situ* measurement. Red line: one-to-one line; yellow line: ordinary least squares linear regression; blue line (and regression equations): reduced major axis linear regression. (B) Locations of the stations with match-ups; (C) and (D) are subsets of match-ups in Bornholm Basin and Gulf of Riga, respectively

period in k_d490 was 0.0023 m^{-1} yr^{-1} (95% confidence range from 0.0014–0.0033) and in Z_{Sd} was –0.037 m yr^{-1} (95% confidence range: –0.051 to –0.024). Both trends are significant (at 95%). The rate of decrease in Z_{Sd} is about 37 cm $decade^{-1}$, which is close to previous estimates using shipboard Z_{Sd} data from earlier periods (Fleming-Lehtinen & Laamanen 2012). However, during the latter part of the satellite time series (2008–2020), there was no significant trend in either k_d490 or Z_{Sd}.

3.3. Combining *in situ* and satellite Z_{Sd} anomaly time series

While matchups of satellite Z_{Sd} retrievals against *in situ* measurements (Fig. 3) did not show a significant mean bias, some bias may still exist for certain areas (e.g. coastal versus offshore), high versus low Z_{Sd} values, or for certain meteorological or oceanographic conditions. An additional source of discrepancy between monthly and annual averages of *in situ* and

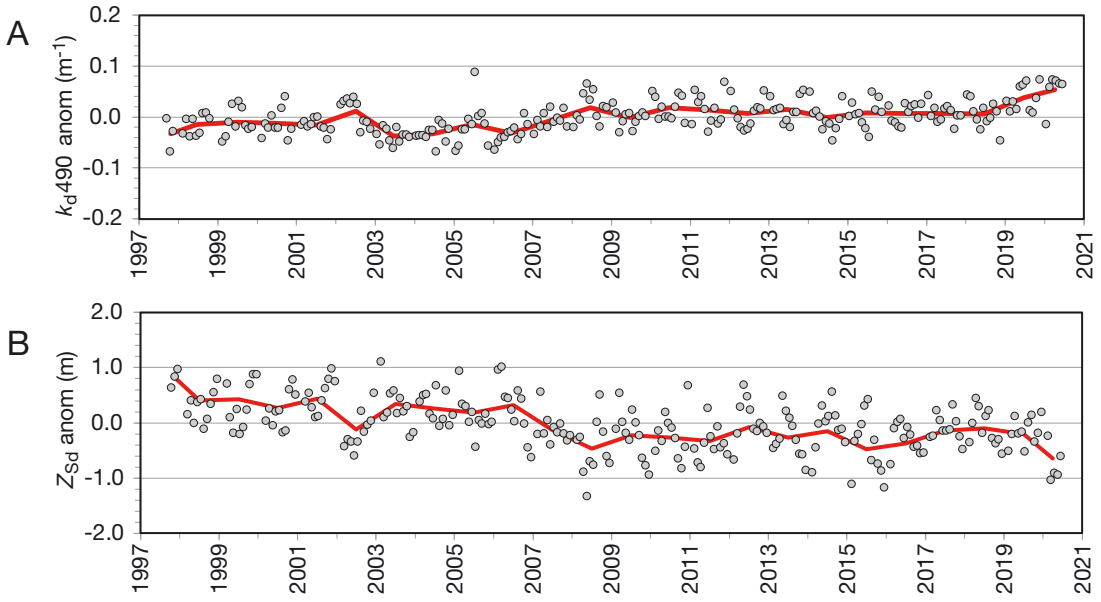

Fig. 4. Time series of the anomalies of (A) satellite-derived coefficient of diffuse attenuation at 490 nm (k_d490) and (B) Secchi depth (Z_{Sd}) in the whole Baltic Sea area (see Fig. 1A). Circles: monthly averages; red lines: annual means. For the full period (1998–2020), the trends of the annual means are increasing for k_d490 (slope = 0.0023 ± 0.009 m^{-1} yr^{-1}) and decreasing for Z_{Sd} (slope = −0.037 ± 0.013 m yr^{-1}). For the later period (2008–2020), the trends are not significant (at 95%)

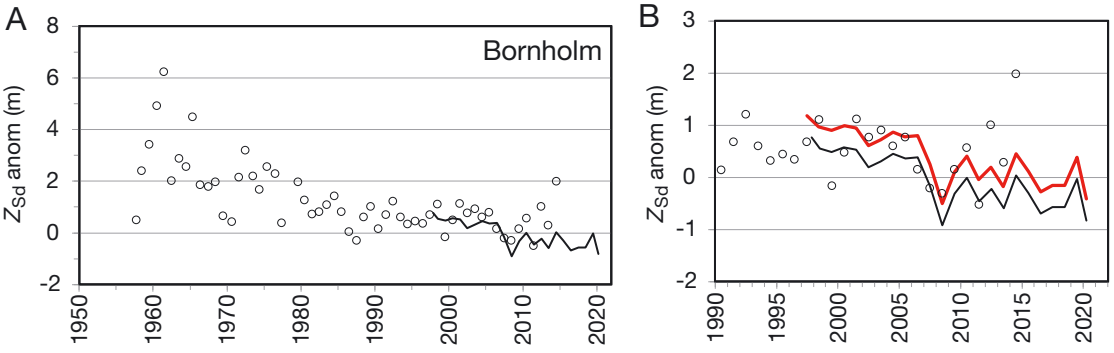

Fig. 5. (A) Time series of Secchi depth (Z_{Sd}) annual anomalies from *in situ* (black open circles) and satellite (black line) observations in the Bornholm Basin. (B) Zoomed region of (A) with the measured satellite (black line) and the mean-adjusted satellite time series (red line; see Section 3.3). In this example, the satellite mean annual values were 0.42 m below the *in situ* annual values. Therefore, 0.42 m was added to the satellite time series (black) to create the mean-adjusted satellite time series (red)

satellite estimates is the difference in sampling pattern and frequency. While satellite averages are based on thousands of pixels that are spread relatively uniformly in space and time (constrained by light and clouds), *in situ* averages are based on relatively small numbers of measurements that are not uniformly distributed in space and time and are likely to be biased compared to the ideal mean. Satellite estimates produce 'cleaner' (i.e. less variable) time series due to a larger number of measurements and allow more reliable trend detection. However, they too are not ideal and contain various errors. The satellite retrieval error and its dependence on various conditions are unknown, and sampling is also limited by clouds and sun elevation. For long-term trend estimates, we need to combine both *in situ* and satellite estimates. When comparing annual averages of *in situ* and satellite Z_{Sd} anomalies (Fig. 5), the satellite-derived annual averages typically appear lower than the *in situ* annual averages. The source of this discrepancy is most likely the difference in sampling patterns but could also be the satellite retrieval bias. In order to make the satellite time series compatible with historic Z_{Sd} data, we

adjusted the satellite time series by their mean bias. We calculated the mean bias between satellite and *in situ* annual averages during the overlapping period in each of the 18 regions and added that to the satellite-derived annual values (Fig. 5). For example, the mean bias during the overlapping period (1997–2014) for the Bornholm Basin annual time series was 0.42 m (satellite underestimation); therefore, 0.42 was added to the satellite-derived time series to create the mean-adjusted satellite time series. The merged annual satellite and *in situ* time series combined *in situ* values (until 1997) with the mean-adjusted satellite values (1998–2020).

3.4. Merged satellite and *in situ* time series of Z_{Sd}

The earliest *in situ* Z_{Sd} data averaged over the whole Baltic Sea area (Fig. 6) showed a puzzling increase of Z_{Sd} anomaly at about 0.29 m yr^{-1} from 1903–1912. We have no explanation for this increase. While the numbers of Secchi disk measurements in the early years were lower than in many later years, there were 216 Z_{Sd} anomaly measurements from 1903–1905 and a total of 829 measurements from 1903–1911. In order to test if the increase in 1903–1912 could have been due to a particular spatial or temporal sampling pattern, we sampled 9 yr of 5 d satellite composites at the same locations and same dates as for the period 1903–1912 but for different sequences of years (1998–2006, 1999–2007,…, 2012–2020). None of the individual time series showed a significant increase, and the estimated slope of the 15 satellite time series was between −0.17 and 0.12 m yr^{-1}. Therefore, we assume that the increase in Z_{Sd} in 1903–1912 was due to unknown natural variability. Regionally, indications of increasing Z_{Sd} from the 1900s to about 1912 can be seen in the East Gotland Basin, West Gotland Basin, and Northern Baltic Proper.

A piecewise linear breakpoint detection analysis (Owens & Wong 2009, Cabanes et al. 2016) applied to the merged satellite–*in situ* time series of 1903–2020 detected 3 breakpoints and 4 segments: a period of increase with a slope of 0.29 m yr^{-1} for 1903–1912 (total change: +2.5 m), a flat period (slope of 0.00 for 1912–1927), a period of significant decrease with a slope of −0.05 for 1927–1987 (total change: −3.24 m), and lastly a period of slight decrease with a slope of −0.01 for 1987–2020 (total change: −0.40 m). The decreasing trend of Z_{Sd} during 1927–2020 estimated with the least squares linear regression had a slope of −0.045 m yr^{-1} (95% confidence limits: −0.051 to −0.039 m yr^{-1}) and resulted in a total decrease of Z_{Sd} by 4.2 m (Table 2) (95% confidence limits: −3.6 to −4.8 m). When calculated for the full period (1903–2020), the slope was −0.032 m yr^{-1} (95% confidence limits: −0.038 to −0.027 m yr^{-1}).

We characterized the long-term dynamics of Z_{Sd} anomaly in the Baltic Sea area and in the 18 HELCOM sub-regions by changes over 3 overlapping periods: the full time series (1903–2020), the period of satellite data availability (1998–2020), and the most recent period after 2008 (Table 2). The full time period may start on a different year, as the start year of the availability of historic Z_{Sd} data was not 1903 for all regions. The *in situ* Z_{Sd} data in the Baltic Sea area showed a drastic decrease until 1986–1987 and no significant change after that. Satellite data starting in 1997/1998 showed a new period of significant decrease from 1997/1998–2008 (Fig. 6). Therefore, while the tapering of the decrease in Z_{Sd} is clear, the start of the recent period of no significant reduction is either 1987 or 2008. Furthermore, in some regions

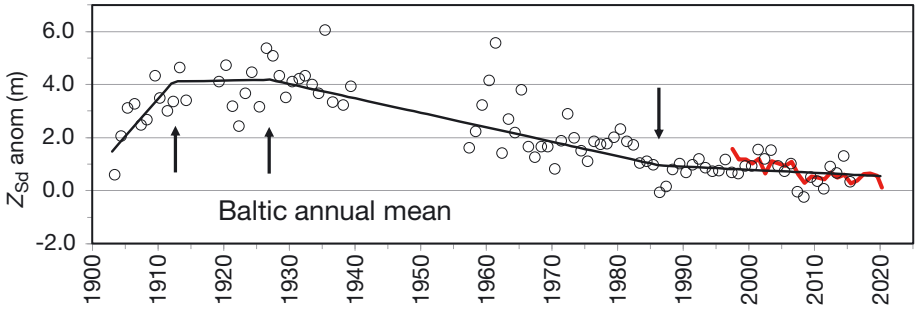

Fig. 6. Time series of the annual Secchi depth (Z_{Sd}) anomaly for the whole Baltic Sea estimated by *in situ* (black open circles) and mean-adjusted satellite (red line) measurements. The merged satellite–*in situ* time series has 3 breakpoints (1912, 1927, and 1987; black arrows) detected with automatic breakpoint detection. The slopes of the 4 segments for the combined satellite–*in situ* data (1903–2020) are 0.29 m yr^{-1} for 1903–1912, 0.00 m yr^{-1} for 1912–1927, −0.05 m yr^{-1} for 1927–1987, and −0.01 m yr^{-1} for 1987–2020

Table 2. Rate of change (slope) in Secchi depth (Z_{Sd}) anomaly (m yr^{-1}) and the total change (m) in different regions of the Baltic Sea. The time period over which the slope was calculated is indicated. **Bold** values are significant at the 95% confidence level. The last column indicates qualitative signs of the trend in the 3 indicated periods; e.g. '– – 0' means negative trends during the first 2 periods and no trend during the last period

Region	Period	Slope (ship + satellite)	Total change in Z_{Sd} (m)	Period	Slope (satellite data only)	1903–2020, 1998–2020, after 2008
Baltic Sea area	1903–2020	**–0.032 ± 0.06**	**–3.8**	1998–2020	**–0.037 ± 0.013**	– – 0
Baltic Sea area	1927–2020	**–0.045 ± 0.06**	**–4.2**	1998–2020	**–0.037 ± 0.013**	– – 0
Kattegat	1906–2020	**–0.016 ± 0.008**	**–1.8**	1998–2020	–0.015 ± 0.024	– 0 0
Great Belt	1907–2020	–0.009 ± 0.011	–1.0	1998–2020	–0.021 ± 0.023	0 0 0
The Sound	1972–2020	–0.019 ± 0.031	–2.1	1998–2020	–0.004 ± 0.019	0 0 0
Kiel Bay	1903–2020	**–0.014 ± 0.008**	**–1.6**	1998–2020	–0.014 ± 0.026	– 0 0
Bay of Mecklenburg	1903–2020	–0.006 ± 0.008	–0.7	1998–2020	**–0.027 ± 0.020**	0 – 0
Arkona Basin	1903–2020	–0.009 ± 0.009	–1.0	1998–2020	**–0.054 ± 0.016**	0 – 0
Bornholm Basin	1903–2020	**–0.021 ± 0.008**	**–2.4**	1998–2020	**–0.056 ± 0.020**	– – 0
Gdansk Basin	1903–2020	–0.005 ± 0.010	–0.6	1998–2020	**–0.042 ± 0.021**	0 – 0
Eastern Gotland Basin	1904–2020	**–0.041 ± 0.011**	**–4.7**	1998–2020	**–0.065 ± 0.021**	– – –
Western Gotland Basin	1907–2020	**–0.047 ± 0.013**	**–5.3**	1998–2020	**–0.041 ± 0.022**	– – 0
Gulf of Riga	1963–2020	**–0.037 ± 0.009**	**–2.1**	1998–2020	–0.004 ± 0.013	– 0 0
Northern Baltic Proper	1906–2020	**–0.044 ± 0.007**	**–4.4**	1998–2020	**–0.069 ± 0.020**	– – –
Western Gulf of Finland	1905–2020	**–0.040 ± 0.007**	**–4.6**	1998–2020	**–0.038 ± 0.020**	– – –
Eastern Gulf of Finland	1905–2020	**–0.028 ± 0.007**	**–3.2**	1998–2020	0.021 ±0.036	– 0 0
Åland Sea	1905–2020	**–0.037 ± 0.007**	**–4.3**	1998–2020	**–0.030 ± 0.016**	– – 0
Bothnian Sea	1905–2020	**–0.037 ± 0.007**	**–4.2**	1998–2020	**–0.041 ± 0.017**	– – –
The Quark	1905–2020	**–0.031 ± 0.007**	**–3.6**	1998–2020	–0.030 ± 0.042	– 0 0
Bothnian Bay	1905–2020	**–0.039 ± 0.007**	**–4.5**	1998–2020	**0.068 ± 0.052**	– + +

the changes did not stop in 2008 (Fig. 7, Table 2). Qualitatively, we can characterize all regions by the signs of change during the 3 periods (full period until 2020, satellite data period 1998–2020, and 2008–2020). For example, Eastern Gotland Basin with '– – –' shows a decrease in all 3 periods but

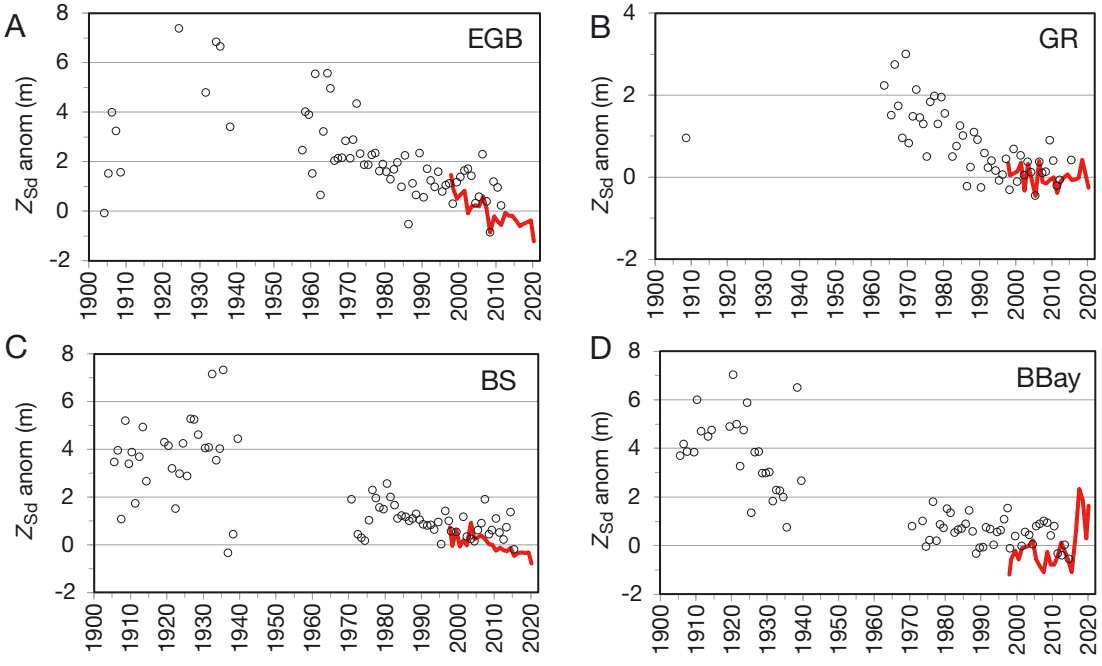

Fig. 7. Time series of Secchi depth (Z_{Sd}) annual anomalies estimated by *in situ* (open circles) and satellite (red line) measurements in (A) Eastern Gotland Basin, (B) Gulf of Riga, (C) Bothnian Sea, and (D) Bothnian Bay (areas shown in Fig. 1B)

Bothnian Bay, with '−++', shows a long-term decrease but an increase during the 2 latest periods (last column of Table 2). In the long term, the Z_{Sd} anomaly decreased significantly in almost all of the sub-areas except the Sound, the Bay of Mecklenburg, and the Arkona Basin, where the change was not statistically significant. In the satellite data period, the decrease in Z_{Sd} was significant in 10 sub-areas and not significant in 7 sub-areas. In only one sub-area, the Bothnian Bay, did Z_{Sd} actually increase during the satellite data period. During the last decade (since ~2008), the long-term decrease in Z_{Sd} had mostly ceased, with a few exceptions. In a group of adjacent areas — the Eastern Gotland Basin, Northern Baltic Proper, Western Gulf of Finland, and Bothnian Sea — the trend of decreasing Z_{Sd} anomaly continued after 2008.

The total decrease in Z_{Sd} over the full measurement period was highest in Western Gotland Basin (−5.3 ± 1.5 m), Eastern Gotland Basin (−4.7 ± 1.3 m), and Western Gulf of Finland (−4.6 ± 0.9 m). The significant increase in Z_{Sd} in the Bothnian Bay after 2016 (Fig. 7D) is either related to some unexplained interannual variability or truly represents an increase in water transparency happening in the Bothnian Bay due to the shorter residence time of the water mass and reduced nutrient loads there (Håkanson & Lindgren 2010). In either case, this location needs further study.

3.5. Spectral k_d anomalies

Increasing k_d490 (Fig. 4A) and decreasing Z_{Sd} (Figs. 4B & 5–7) are evidence that the water transparency in the Baltic Sea has been decreasing, most likely at least since the 1920s. However, what is not clear are the primary factors causing the decrease in water transparency. We can get some clues by comparing the rates of change (m^{-1} yr^{-1}) of the different spectral bands of k_d. Values of k_d were computed at 6 spectral bands (412, 443, 490, 510, 560, 665 nm) according to Lee et al. (2015). While satellite data for these calculations are available from late 1997–2020, early data (1997–2002) were only available from a single sensor (SeaWiFS). It appeared that the early period was noisy, probably due to the lower signal-to-noise ratio of SeaWiFS compared to other sensors (Hu et al. 2012). We therefore estimated the trends in spectral k_d for the period 2003–2020, when merged data from 3–4 satellite sensors were available (Fig. 8). While these estimates show the different

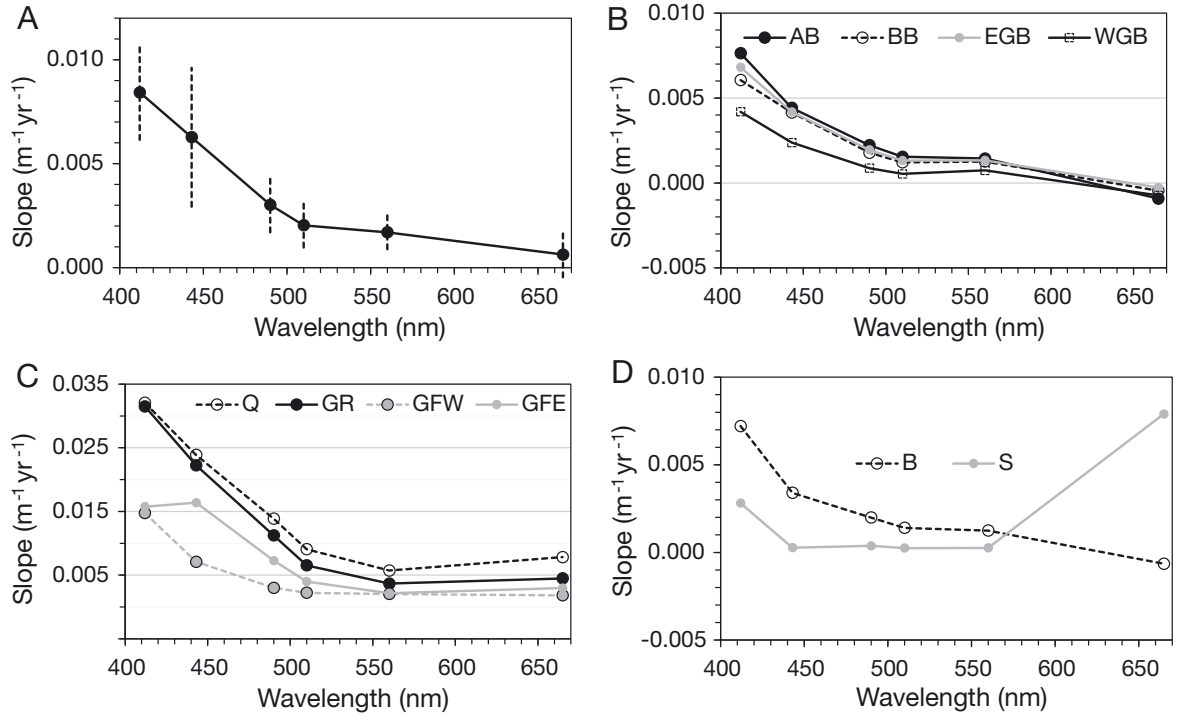

Fig. 8. Slope of the linear change in time of the spectral light attenuation coefficient for the 6 wavelengths in the Baltic Sea in different regions (2003–2020): (A) Baltic Sea area (with 95% confidence limits); (B) Arkona Basin (AB), Bornholm Basin (BB), Eastern Gotland Basin (EGB), and Western Gotland Basin (WGB); (C) The Quark (Q), Gulf of Riga (GR), Gulf of Finland West (GFW), and Gulf of Finland East (GFE); and (D) Great Belt (B) and the Sound (S)

rates of change in different spectral bands of light during the last 18 yr (2003–2020), they do not necessarily mean that similar rates of change applied to earlier periods. When averaged over the whole Baltic Sea, k_d has increased in all spectral bands, but the change has been most rapid at 412 nm, followed by 443 nm (Fig. 8A). While the confidence limits are rather wide, particularly at 443 nm, the shapes of the rates of spectral increases in k_d were similar in most regions of the Baltic with only slight variations (Fig. 8B). The highest rates of change were observed in the Quark and Gulf of Riga, followed by the Gulf of Finland (Fig. 8C). In contrast to the Western Gulf of Finland and most other areas, the Eastern Gulf of Finland showed the fastest rate of change in the 443 nm band, indicating a growing role of phytoplankton (Fig. 8C). Surprising differences were observed between the Danish straits, with the Sound showing the fastest rate of change in the 665 nm band (Fig. 8D). In conclusion, in most areas, the increase in light attenuation has been strongest in the 412 nm band, affected primarily by chromophoric dissolved organic matter (CDOM), whereas in the eutrophic Eastern Gulf of Finland the increase in the absorption by phytoplankton in the 443 nm band has been the strongest.

Our analysis shows that the k_d minimum in the Baltic Sea is almost exclusively in the 560 nm band and only rarely switches to the 510 nm band (in offshore Bornholm and Gotland basins) before the phytoplankton spring bloom in February–March.

4. DISCUSSION

Water transparency is an important habitat characteristic for all aquatic organisms that are affected by the optical environment (Dupont & Aksnes 2013). The utility of water transparency data is further increased by the availability of long records of Z_{Sd}, which makes it possible to assess changes in the marine environment over more than a century. Such long time series are not available for other water quality indicators. An important advantage of satellite estimates of water transparency or water clarity is the large-scale and frequent coverage of those measurements. The potentially operational nature and near real-time availability of satellite data is crucial for applications such as commercial and recreational diving (Prasad et al. 1998). Satellite measurements provide large numbers of spatial and temporal samples that result in 'cleaner' (i.e. less variable) time series, allowing more reliable change detection. As a disadvantage, satellite-based ocean color sensors are limited to high light and clear weather conditions, which makes them unavailable during cloudy periods and in the winter season over most of the Baltic.

As noted by Dupont & Aksnes (2013), irregular locations of Z_{Sd} measurements can introduce false trends in Z_{Sd} data, e.g. due to sampling being biased towards more near-shore or more offshore locations. To reduce such bias, we normalized the *in situ* Z_{Sd} by subtracting the satellite-derived space and seasonal mean (climatology). Such normalized values, i.e. Z_{Sd} anomalies, are expected to make different areas and time periods more comparable. However, such normalization does not remove variability due to the small-scale spatial and temporal variability.

The relatively low spatial resolution (~4.5 km) of the satellite data used here is sufficient for characterization of the Baltic Sea and its major basins but not for the smaller bays and inlets. Increasing the spatial resolution to 1 km is straightforward with most ocean color sensors and even to 350 m (OLCI) or 250 m (SGLI) while applying the same algorithm. A method extending the Lee et al. (2015) Z_{Sd} algorithm to the high-resolution satellite sensors with different spectral bands (OLI: 30 m on Landsat; MSI: 10 m on Sentinel-2) was recently developed by Pitarch & Vanhellemont (2021). Ship-borne sampling is expensive and time-consuming and may not represent the spatial and temporal variability near the coast. Instead of ships, automated measurements from sensors mounted on BGC-Argo floats (Jemai et al. 2021) or buoys can provide high-resolution time series to resolve that variability.

The trend of decreasing water transparency in the Baltic Sea has been demonstrated in several previous studies (Launiainen et al. 1989, Sandén & Håkansson 1996, Fleming-Lehtinen & Laamanen 2012, Dupont & Aksnes 2013) and is related to increased nutrient loads (e.g. Fleming-Lehtinen & Laamanen 2012). Our trend estimates for the whole Baltic Sea from the merged shipborne–satellite time series of about −0.04 m yr^{-1} are close to previous estimates. The trend from satellite data alone (1998–2020) was −0.037 m yr^{-1}. We have no explanation for the observed increase in the average Z_{Sd} in the Baltic Sea from 1903 to the mid-1920s. The tapering of the Z_{Sd} decreasing trend after 1987 is evident in some areas and has also been noted before (Fleming-Lehtinen & Laamanen 2012). The timing of the flattening of the Z_{Sd} trend is not certain. While satellite data (1998–2020) show no significant change after 2008, earlier *in situ* data show flattening of the trend already after 1986–1987, i.e. before the availability of

satellite data. This is probably related to multi-year fluctuations in Z_{Sd} caused by changes in river inflows, winds, currents, and other factors. The period 1986–1987 with Z_{Sd} minima was also notable for an almost complete absence of cyanobacteria accumulations (Kahru & Elmgren 2014) due to cold and rainy summers. While the decrease in Z_{Sd} in the Baltic Sea area and most of its sub-regions ceased at about 2008, the decrease continued even after that in some central Baltic Sea regions (Eastern Gotland Basin, Northern Baltic Proper, Western Gulf of Finland, and Bothnian Sea).

Satellite-detected changes in spectral light attenuation indicate that the strongest increase has been in bands affected by light absorption by CDOM (412 nm) and phytoplankton (443 nm). While Z_{Sd} is determined by light attenuation in the maximum transparency window (560 nm band in the Baltic Sea), the increase in CDOM and phytoplankton concentrations also gives an increase in k_d at 560 nm that reduces Z_{Sd}. We can therefore conclude that the decadal decrease in Z_{Sd} in the Baltic Sea was caused primarily by a combination of increasing CDOM and phytoplankton biomass.

5. CONCLUSIONS

A method of normalizing sparse historic shipboard measurements with modern satellite data was applied to a large archive of *in situ* measurements of Z_{Sd} in the Baltic Sea. Time series of the merged *in situ*–satellite estimates for 1927–2020 showed a trend of decreasing Z_{Sd} with a mean slope of −0.045 ± 0.06 m yr^{-1}. The mean Z_{Sd} decreased from 1927–2020 by 4.2 ± 0.6 m. While the decreasing trend has tapered off in most areas, the decrease in Z_{Sd} is still continuing in several major regions. During the period of satellite observations, light attenuation has increased the most in the spectral bands affected predominantly by CDOM (412 nm) and phytoplankton (443 nm).

Acknowledgements. Satellite data were provided by the ESA OC-CCI project (https://esa-oceancolour-cci.org/). This work was supported by the Leibniz Institute for Baltic Sea Research Warnemünde (IOW) while M.K. was a visiting scientist. We thank Susanne Kratzer for helpful discussions and some match-up data.

LITERATURE CITED

Aarup T (2002) Transparency of the North Sea and Baltic Sea — a Secchi depth data mining study. Oceanologia 44: 323–337

Alikas K, Kratzer S (2017) Improved retrieval of Secchi depth for optically-complex waters using remote sensing data. Ecol Indic 77:218–227

Cabanes C, Thierry V, Lagadec C (2016) Improvement of bias detection in Argo float conductivity sensors and its application in the North Atlantic. Deep Sea Res I 114: 128–136

Dupont N, Aksnes DL (2013) Centennial changes in water clarity of the Baltic Sea and the North Sea. Estuar Coast Shelf Sci 131:282–289

Elmgren R (1989) Man's impact on the ecosystem of the Baltic Sea: energy flows today and at the turn of the century. Ambio 18:326–332

Fleming-Lehtinen V, Laamanen M (2012) Long-term changes in Secchi depth and the role of phytoplankton in explaining light attenuation in the Baltic Sea. Estuar Coast Shelf Sci 102–103:1–10

Fonselius SH (1969) Hydrography of the Baltic deep basins. III. Series Hydrography, Vol 23. Fishery Board of Sweden, Lund

Håkanson L, Lindgren D (2010) Water transport and water retention in five connected subbasins in the Baltic Sea — simulations using a general mass-balance modeling approach for salt and substances. J Coast Res 26:241–264

HELCOM (2018) State of the Baltic Sea — second HELCOM holistic assessment 2011–2016. Baltic Sea Environment Proceedings 155. Baltic Marine Environment Protection Commission, Helsinki

Hu C, Feng L, Lee L, Davis CO, Mannino A, McClain CR, Franz BA (2012) Dynamic range and sensitivity requirements of satellite ocean color sensors: learning from the past. Appl Opt 51:6045–6062

Jemai A, Wollschläger J, Voß D, Zielinski O (2021) Radiometry on Argo floats: from the multispectral state-of-the-art on the step to hyperspectral technology. Front Mar Sci 8:676537

Kahru M, Elmgren R (2014) Multidecadal time series of satellite-detected accumulations of cyanobacteria in the Baltic Sea. Biogeosciences 11:3619–3633

Kahru M, Elmgren R, Savchuk O (2016a) Changing seasonality of the Baltic Sea. Biogeosciences 13:1009–1018

Kahru M, Lee Z, Mitchell BG, Nevison CD (2016b) Effects of sea ice cover on satellite-detected primary production in the Arctic Ocean. Biol Lett 12:20160223

Launiainen J, Pokki J, Vainio J, Niemimaa J, Voipio A (1989) Long-term changes in the Secchi depth in the northern Baltic Sea. In: XIV Geofysikan päivät, Helsinki, 3–4 May 1989. Geophysics Society, Helsinki, p 117–121 (in Finnish, with English Abstract)

Lee Z, Shang S, Hu C, Du K and others (2015) Secchi disk depth: a new theory and mechanistic model for underwater visibility. Remote Sens Environ 169:139–149

Lee Z, Shang S, Du K, Wei J (2018) Resolving the long-standing puzzles about the observed Secchi depth relationships. Limnol Oceanogr 63:2321–2336

Liu X, Meng X, Wang X, Bi D, Chen L, Lou Q (2020a) Using a semi-analytical model to retrieve Secchi depth in coastal and estuarine waters. Acta Oceanol Sin 39: 103–112

Liu Y, Chenchao X, Li J, Zhang F, Wang S (2020b) Secchi disk depth estimation from China's new generation of GF-5 hyperspectral observations using a semi-analytical scheme. Remote Sens 12:1849

Owens WB, Wong APS (2009) An improved calibration method for the drift of the conductivity sensor on

autonomous CTD profiling floats by θ–S climatology. Deep Sea Res I 56:450–457

Pitarch J, Vanhellemont Q (2021) The QAA-RGB: a universal three-band absorption and backscattering retrieval algorithm for high resolution satellite sensors. Development and implementation in ACOLITE. Remote Sens Environ 265:112667

Prasad KS, Bernstein RL, Kahru M, Mitchell BG (1998) Ocean color algorithms for estimating water clarity (Secchi depth) from SeaWiFS. J Adv Mar Sci Technol Soc 4: 301–306

Preisendorfer RW (1986) Secchi disk science: visual optics of natural waters. Limnol Oceanogr 31:909–926

Sandén P, Håkansson B (1996) Long-term trends in Secchi depth in the Baltic Sea. Limnol Oceanogr 41:346–351

Sathyendranath S, Brewin R, Brockmann C, Brotas V, Calton B, Chuprin A, Platt T (2019) An ocean-colour time series for use in climate studies: the experience of the ocean-colour climate change initiative (OC-CCI). Sensors (Basel) 19:4285

Savchuk OP (2018) Large-scale nutrient dynamics in the Baltic Sea, 1970–2016. Front Mar Sci 5:95

Shang S, Lee Z, Shi L, Lin G, Wei G, Li X (2016) Changes in water clarity of the Bohai Sea: observations from MODIS. Remote Sens Environ 186:22–31

York D, Evensen NM, Martinez ML, Delgado JD (2004) Unified equations for the slope, intercept, and standard errors of the best straight line. Am J Phys 72:367–375

Editorial responsibility: Katherine Richardson, Copenhagen, Denmark
Reviewed by: E. Boss, S. Markager and 3 anonymous referees

Submitted: January 7, 2022
Accepted: July 29, 2022
Proofs received from author(s): September 16, 2022